Systematic study of sol-gel parameters on TiO_2 coating for CO_2 photoreduction

Warren Athol Thompson*, Clement Perier, M. Mercedes Maroto-Valer

Research Centre for Carbon Solutions (RCCS), School of Engineering & Physical Sciences, Heriot-Watt University, Edinburgh, EH14 4AS, UK

ARTICLE INFO

ABSTRACT

An optimized sol-gel method for TiO_2 coating was developed for CO_2 photoreduction using a systematic Design of Experiments (DOE) approach and an efficient Plackett-Burman (PB) design. Conducting fifteen experiments, the effects of seven sol-gel process parameters were investigated on four catalytic properties for CO_2 photo-reduction: band gap, catalyst coverage, anatase crystallinity and ratio anatase:rutile. The PB design results yielded a wide range for the catalyst's properties: band gap (1.86–3.35 eV), coverage (11.53–99.63%), anatase crystallinity (0–48.5 nm) and ratio anatase:rutile (1:0 and 0:1). Machine vision using manual global, Otsu global and adaptive thresholding were compared for estimating the coverage of catalyst on a glass slide support.

1. Introduction

CO_2 photoreduction is a promising route towards lowering CO_2 emissions and potentially producing useful chemicals that include CH_4 as a fuel [1,2]. TiO_2 and its derivatives have often been used for the photoreduction of CO_2 due to its band gap, low cost, availability and chemical stability [3,4]. The efficiency of CO_2 photoreduction using TiO_2 can be effected by the catalyst's properties: band gap [3], crystallinity [3,5] and ratio of anatase:rutile phases [6]. The band gap of TiO_2 prepared by sol-gel has been previously modified using phosphorous dopants [7], nitrogen and fluorine dopants [8], addition of SiO_2 to N-doped TiO_2 and calcination temperature [9,10]. The crystallinity of TiO_2 particles isolated from sol-gel have been tuned by calcination holding time [11] and calcination temperature [9,10,12–16]. The effect of calcination temperature on the ratio of anatase:rutile also has been reported [9,10,17–22].

For the practical application of CO_2 photoreduction and flexibility in reactor design, bearing in mind the challenge of dealing with light with directional limitations as an energy source, the catalyst needs to be applied to a support to yield a quality coating. TiO_2 coating by sol-gel is attractive, as it requires a simple set up and is relatively low cost. Films of TiO_2 have been prepared using sol-gel dip coating and spin coating methods [9,10,12,23–26]. Sol-gel preparation parameters have been previously studied, including amount of water, solvent, acidic hydrolyzing catalyst, high molecular weight co-polymer, calcination temperature and holding time. However, there is no example that includes a detailed investigation of all the parameters used in the preparation of

a TiO_2 sol-gel on the catalyst's properties: band gap, crystallinity, ratio anatase:rutile and coating quality. This is most likely the case as sol-gel procedures have several preparation parameters and it would require a large number of experiments to investigate each parameter's effect on each property. In addition, using published work and consolidating them into a single experiment that yields all of the desired properties for CO_2 photoreduction is implausible, due to the variation in reagents, catalysts, experimental settings and setups used.

Design of Experiments (DOE) is a powerful tool that allows for generating efficient systematic experimental designs to screen and optimise parameters on selected responses or in this case catalyst properties. DOE is an efficient tool for optimising yield for the synthesis of catalysts and catalytic processes; a variety of examples using full factorial, central composite and Box-Behnken designs are described in the literature [27–33]. The preparation of thin films for novel materials and catalytic processes are challenging, as they require the investigation and optimisation of several process parameters. DOE offers a robust and systematic method for investigating and optimising these coating parameters. A D-optimal design was successfully employed for the development of inkjet printed electrochromic thin films [34]. The effect of parameters for the preparation of TiO_2 thin films: amount acetic acid, water, ethanol, co-polymer Pluronic P123 and calcination temperature on the activity of photodegradation of methyl orange was investigated using a Taguchi method [35]. In another example, the preparation of TiO_2 powder by sol-gel process, a full factorial design was used to investigate the effect of the parameters (amount Titanium tetra-isopropoxide, water, hydrochloric acid and flow feeding rate of reactants) on

---

Table 1

Experiments performed using PB design. For the ratio anatase and crystallinity response, extra experiments were performed to replace the low experimental points from 250 to 400 °C and the three midpoints from 450 to 525 °C. This was done as at 250 °C, no response could be recorded as the resulting sol-gel was amorphous.

Std. Order	Sample name	Sol-gel preparation				Calcination conditions		
		IPA (ml)	Acetic (ml)	Water (ml)	PPG (ml)	Calcination Temp (°C)	Calcination Rate (°C. min^{-1})	Hold Time (min)
1	WT1	3.0	0.010	0.6400	0.6	250	1	120
9	WT2	0.6	0.010	0.0032	3.0	650	15	10
11	WT3	0.6	0.100	0.0032	0.6	250	15	120
4	WT4	3.0	0.010	0.6400	3.0	250	15	10
15	WT5	1.8	0.055	0.3216	1.8	450	8	65
2	WT6	3.0	0.100	0.0032	3.0	250	1	10
8	WT7	0.6	0.010	0.6400	3.0	650	1	120
5	WT8	3.0	0.100	0.0032	3.0	650	1	120
12	WT9	0.6	0.010	0.0032	0.6	250	1	10
3	WT10	0.6	0.100	0.6400	0.6	650	1	10
6	WT11	3.0	0.100	0.6400	0.6	650	15	10
14	WT12	1.8	0.055	0.3216	1.8	450	8	65
13	WT13	1.8	0.055	0.3216	1.8	450	8	65
10	WT14	3.0	0.010	0.0032	0.6	650	15	120
7	WT15	0.6	0.100	0.6400	3.0	250	15	120

the mean particle size of calcined TiO_2 isolated [36].

In this work, a systematic approach using DOE is presented to screen and optimise seven variables: amount isopropanol (IPA), acetic acid, water and polypropylene glycol (PPG), calcination temperature, heating ramp and holding time in fifteen experiments (Table 1). A subset design of DOE, a Plackett-Burman (PB) was used, as it is very efficient at screening four or more parameters in as few as fifteen experiments. To the author's knowledge, this is the first example of a very efficient Plackett-Burman design being used for the process development and investigation of the effect of seven sol-gel preparation parameters on several photocatalytic and physical properties of TiO_2 for CO_2 photoreduction.

2. Experimental

2.1. DOE

Minitab 17 Statistical Software (2010). [Computer software]. State College, PA: Minitab, Inc. (www.minitab.com) was used for creating the experimental design points (Table 1) and analysing the design's responses (Table 2). Minitab was used to model each parameters effect on a response by fitting a linear function to the parameters under investigation to a response, with Eq. (1) showing a general form of the linear function. The error residual function is shown by Eq. (2).

$$Y = \beta_0 + \beta_i X_i + \varepsilon_i \tag{1}$$

$$\varepsilon_i = y - (\beta_0 + \beta_i X_i) \tag{2}$$

where: Y, y is the fitted response and actual response values respectively β_0 is the y-axis intercept ε_i is the error residual X_i is the matrix of parameter values, n is the number of parameters β_i is the co-efficient of the parameter calculated form the cost function $i = 1,…,$ for n parameters

The parameter coefficients (β) and error term (ε) were determined from a cost function that minimizes the error residual (ε) between the actual response value and fitted response (Y) by a least squares method Eq. (3).

$$\text{Find } \beta_0, \beta_i, \text{ Min} \sum_{i}^{n} (\varepsilon_i)^2 = \sum_{i}^{n} (Y_i = y_i)^2 \tag{3}$$

Parameters coefficients were significant if the value is shown to be statistically not equal to zero. This was determined by analysis of variance (ANOVA), by calculating the p-value with the null hypothesis that

Table 2

Experimental results using a PB design for band gap, catalyst on support coverage, crystallinity of anatase and ratio of anatase and rutile phases

Run Order Sample name	Band gap (eV)	Coverage (%)	Anatase Crystallinity (nm)	Ratio anatase phase (F_A)	Ratio rutile phase (F_R)
WT1	2.10	30.94[a]	5.08	1.00	0.00
WT2	3.35	98.94[b]	28.01	0.75	0.25
WT3	1.77	67.31[a]	6.67	1.00	0.00
WT4	2.34	55.74[a]	0.99	1.00	0.00
WT5	3.13	22.55[a]	16.13	1.00	0.00
WT6	2.70	99.63[b]	2.06	1.00	0.00
WT7	3.25	18.25[a]	30.22	1.00	0.00
WT8	3.22	52.35[a]	48.15	0.06	0.94
WT9	2.17	90.84[a]	ND	ND	ND
WT10	3.20	11.53[a]	19.44	1.00	0.00
WT11	3.21	23.34[a]	22.46	0.93	0.07
WT12	3.15	23.47[a]	14.17	1.00	0.00
WT13	3.24	23.06[a]	16.23	1.00	0.00
WT14	3.30	37.41[a]	0.00	0.00	1.00
WT15	1.86	76.59[b]	8.45	1.00	0.00

[a] Otsu global thresholding.
[b] Adaptive thresholding and ND = Amorphous material, no data collected by XRD.

the parameter coefficient was equal to zero. The null hypothesis was rejected if the p-value was less than the significance level (alpha, α). The terms were systematically removed from the linear model starting with the parameter coefficient with largest p-value. If three or less parameters were significant, the model was converted to a full factorial design, that possibly included interaction terms in the linear model. Interactions are difficult to show experimentally and indicate if parameters effects are influenced by other parameter settings.

The effect of the parameters were investigated on the responses: band gap, coverage, crystallinity and phase ratio of anatase:rutile (Table 2). The models presented were compared to the literature and consolidated to yield a single experimental point using a single coating procedure that yielded a desirable response for band gap, crystallinity, ratio of anatase:rutile and coating coverage. The best design point was further optimized by adjusting the PPG volume equivalents. The use of lower cost lower molecular weights PPG were investigated. The optimized procedure was used to coat stainless steel mesh supports and benchmarked with P25 TiO_2.

2.2. Materials preparation

Isopropanol (IPA, 99.96%) and glacial acetic acid (99.7%) were purchased from Fisher Chemical. Titanium (IV) n-butoxide (99%, Acros), 400, 1000 and 3000 g.mol^{-1} polypropylene glycol (PPG, Alfa Aesar) were purchased from the commercial suppliers shown in brackets. The deionized water used was from a Merck Direct-q deionizer.

2.2.1. Preparation of TiO$_2$ sol-gel

Sol-gel mixtures were prepared using different amounts of chemicals as listed in Table 1. 0.6 ml of titanium (IV) n-butoxide was used for all of the experiments. IPA, titanium butoxide and glacial acetic acid were transferred and agitated together in a sealed sample vial. Deionized water was added in a single step and the vial sealed.

To ensure homogeneity, of at times a viscous mixture, the mixture was agitated for eighty minutes. The mixture was stored in a sealed vial to age overnight. PPG was then added in a single step before being agitated for 40 min. Samples were stored in a fridge set at 4 °C for a maximum period of one month, to prevent excessive ageing, before being used to coat a glass strip support. Additional experiments were carried out using the same procedure described above for WT2 (Table 1) towards testing the effect of molecular weight (400, 1000 and 3000 g.mol^{-1}) and volume equivalents of PPG on the sol-gel.

2.2.2. Coating and calcination

Glass strips (15 of 0.5 mm × 25 mm) were cleaned with dilute sulphuric acid in water (10%), rinsed with deionized water washes (3 × 25 ml) and one IPA wash (25 ml). The glass strips were then dried overnight in an oven at 70 °C. Approximately 2.5 ml of the sol-gel prepared was transferred to a HPLC sample vial. The glass strips were immersed into the sol-gel for one minute before being withdrawn using a dip coater motor set at 50 Hz (Te-Sun Industry Works, Taiwan). The coated glass strips and an aliquot of the sol-gel prepared were calcined as shown in Table 1. For CO$_2$ photoreduction tests, stainless steal gauge 20 mesh was coated using a similar procedure described above for the glass strips without a dilute sulphuric acid wash.

2.3. Sample characterization

2.3.1. UV-vis absorption

The light absorption and electronic band were characterized using a UV–vis spectrometer (Perkin Elmer lamda 950) equipped with a 150 mm integration sphere (Perkin Elmer). The band gap was determined using a direct intercept method (Fig. 2) to estimate the adsorption maxima which was then used in Eq. (4) [37,38].

$$E_g = \frac{h \times \frac{c}{\lambda}}{C_f} \tag{4}$$

where: E_g is the band gap (eV)h is Planck's constant (6.626 × 10^{-34} m^2 kg s^{-1})c is the speed of light (3.00 × 10^8 m s^{-1})λ is the wavelength of adsorption (m)C_f is the conversion factor (1.6 × 10^{-19} J)

2.3.2. Image analysis

The coated slides and coverage were analyzed by scanning electron microscopy (SEM) and Energy-dispersive X-ray spectroscopy (EDX). A Quanta FEG 650 SEM equipped with Oxford Instruments X-max^{N}150 EDX detector and a XL30 LaB^{6}ESEM equipped with Oxford Instruments X-max 80 EDX detector operated under low vacuum (Typically 0.8 Torr) were used.

2.3.3. Crystallinity and phase analysis

Powder X-ray diffraction to determine crystallinity and anatase:rutile phase ratio was performed using a Bruker D8 Advance powder diffractometer, operating with Ge-monochromated Cu K-alpha

radiation (wavelength = 1.5406 Å) and a LynxEye linear detector in reflectance mode. Data were collected over the angular range 5–85 degrees in two-theta in one hour. The Debye-Scherrer equation was used to approximate the crystallite size using the half width maximum height of the most intense peak for the anatase and or rutile phase from the XRD pattern and Eq. (5) [39].

$$D = \frac{K * \lambda}{\beta * \cos(\theta)} \tag{5}$$

where:

d is the crystallite size (nm)

K is the dimensionless shape factor

β is the full width at half maximum (FWHM) intensity of the (1 0 1) peak (rad)

θ is Bragg's diffraction angle (°)

The ratio between anatase and rutile phases was calculated using XRD peak intensity values for anatase and rutile with the Spurr and Myers equation Eq. (6) [40].

$$f_A = \frac{1}{\left(1 + 1.265 \frac{I_R}{I_A}\right)} \tag{6}$$

where:

f_A is the fraction of anatase phase in the powder

I_A and I_R are the X-ray intensities of the anatase (101) and rutile (110) diffraction peaks, respectively

2.3.4. Surface area, pore volume and CO$_2$ adsorption capacity

Samples were degassed under a constant purge of N$_2$ at 200 °C for 10 h. The surface area of the optimised samples were estimated by N$_2$ adsorption isotherms measured at 77 K over forty equidistant points from 0 – 0.95 P/P$_0$ (Gemini VII 2390). The Brunauer, Emmett and Teller (BET) method was used to estimate the surface area from the N$_2$ adsorption isotherms by fitting a straight line to the data collected between 0.05 – 0.3 P/P$_0$ [41]. The pore volume was measured at the single point of 0.95 P/P$_0$ [41]. CO$_2$ adsorption capacities were estimated by the maximum value found from the CO$_2$ adsorption isotherm measured at 273 K over forty equidistant points from 0 to 0.95 P/P$_0$ (Gemini VII 2390).

2.4. CO$_2$ photoreduction tests

CO$_2$ photoreduction tests using coated stainless steel gauge 20 mesh were analyzed by an online gas chromatography (GC). A GC (Agilent, Model 7890B series) with a Hayesep Q column (1.5 m), 1/16 inch od, 1 mm id), MolSieve 13X (1.2 m), 1/16 inch od, 1 mm id), thermal conductivity detector, nickel catalyzed methaniser and flame-ionization detector was used to analyze the samples every four minutes. The experimental rig used is shown in Fig. 1. A flow rate of 0.063 ml.min^{-1} CO$_2$ was sent through a bubbler 20 ± 2.0 °C to the reactor overnight to purge the system and saturate the catalyst surface with the reagent gases. The reaction was performed at 36 ± 0.1 °C. A UV lamp was used as the light source, light intensity was set at 75 mW.cm^{-2} with a wavelength of 365 nm. For comparison to P25 TiO$_2$, stainless steel gauge 20 mesh was coated with P25 via a slurry deposition of P25 and IPA in an ultrasound bath. The coated mesh was then dried at 150 °C for 2 h.
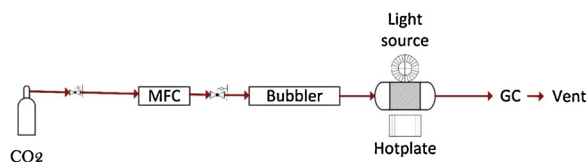

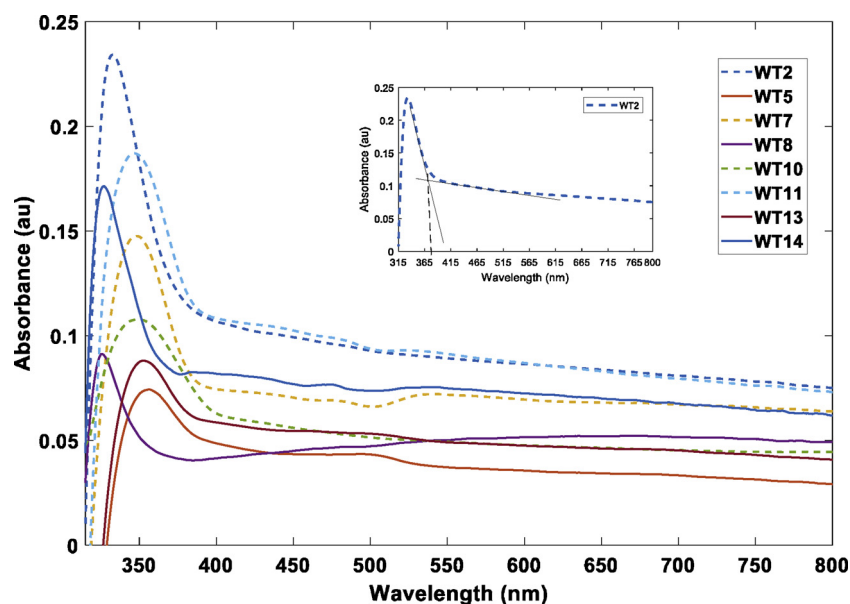**Fig. 1.** Experimental rig used for CO$_2$ photoreduction tests.

Fig. 2. Representative UV–vis absorption plots for the PB samples that yielded bandgaps between 3.13–3.35 eV. The boxed figure is an example of the direct intercept method used to estimate the band gap for WT2. The UV–vis absorption raw data for all fifteen PB experiments can be accessed in the supplementary section.
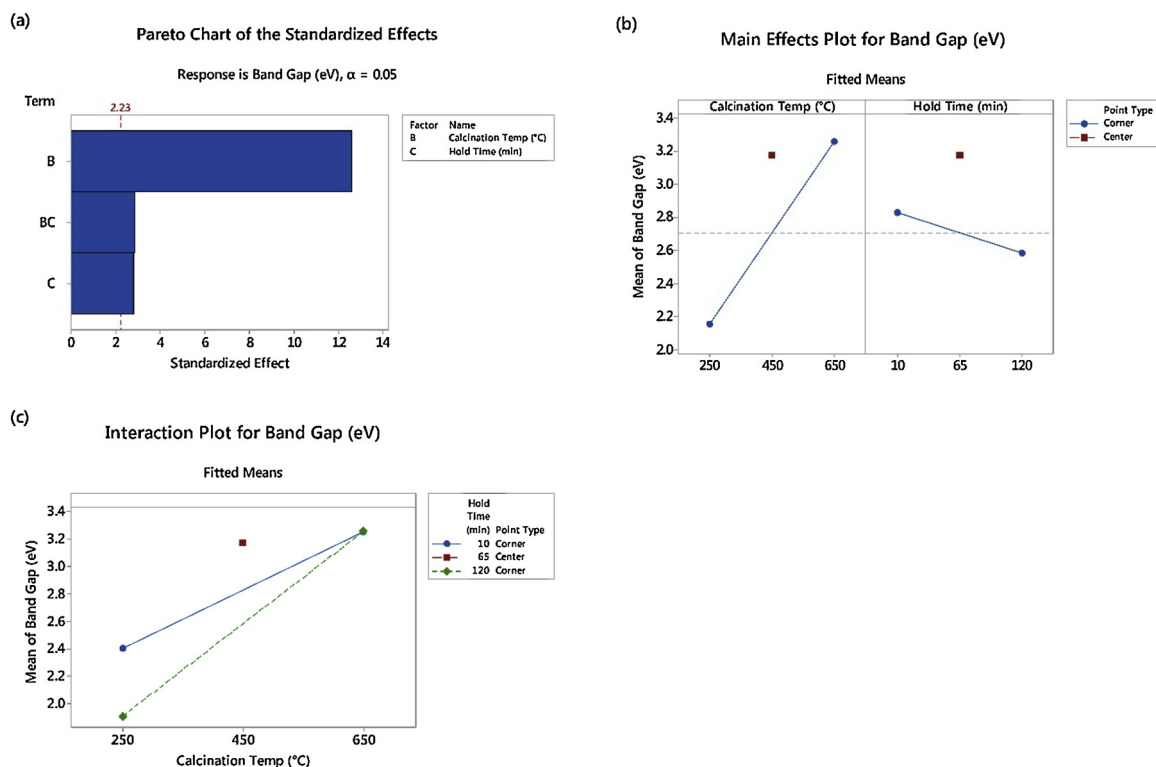

Fig. 3. (a) Pareto chart of effects showing significance of calcination temperature, holding time and their interaction on the band gap response. (b) Main effects plot showing effect of calcination temperature and holding time. (c) Interaction effect between calcination temperature and holding time.

3. Results and discussion

3.1. PB design results

3.1.1. Interpreting DOE charts

Pareto charts of standardized effects, main effects and interaction plots are powerful visualization tools that show visually the results of the PB design. Pareto charts of standardized effects indicate the statistically significant parameters as those that are above the red reference line. The weight of the parameters is also indicated by the length of the plotted bar. The main effects plot indicates the parameters effect between high and low settings. The blue circles (Corner point type) on either side of the line is the mean of the values recorded for the high and low settings. The blue line connects these two points. A line with a steep slope indicates the parameter has a strong effect on the response. The red square indicates the mean of the center points (Center point type) – for this study, three replicate points were performed. The grey dotted line indicates the mean for all of the experiments. An interaction plot has similar features to a main effects plot, but includes the presence of an interaction by two intersecting non-parallel lines. The blue solid
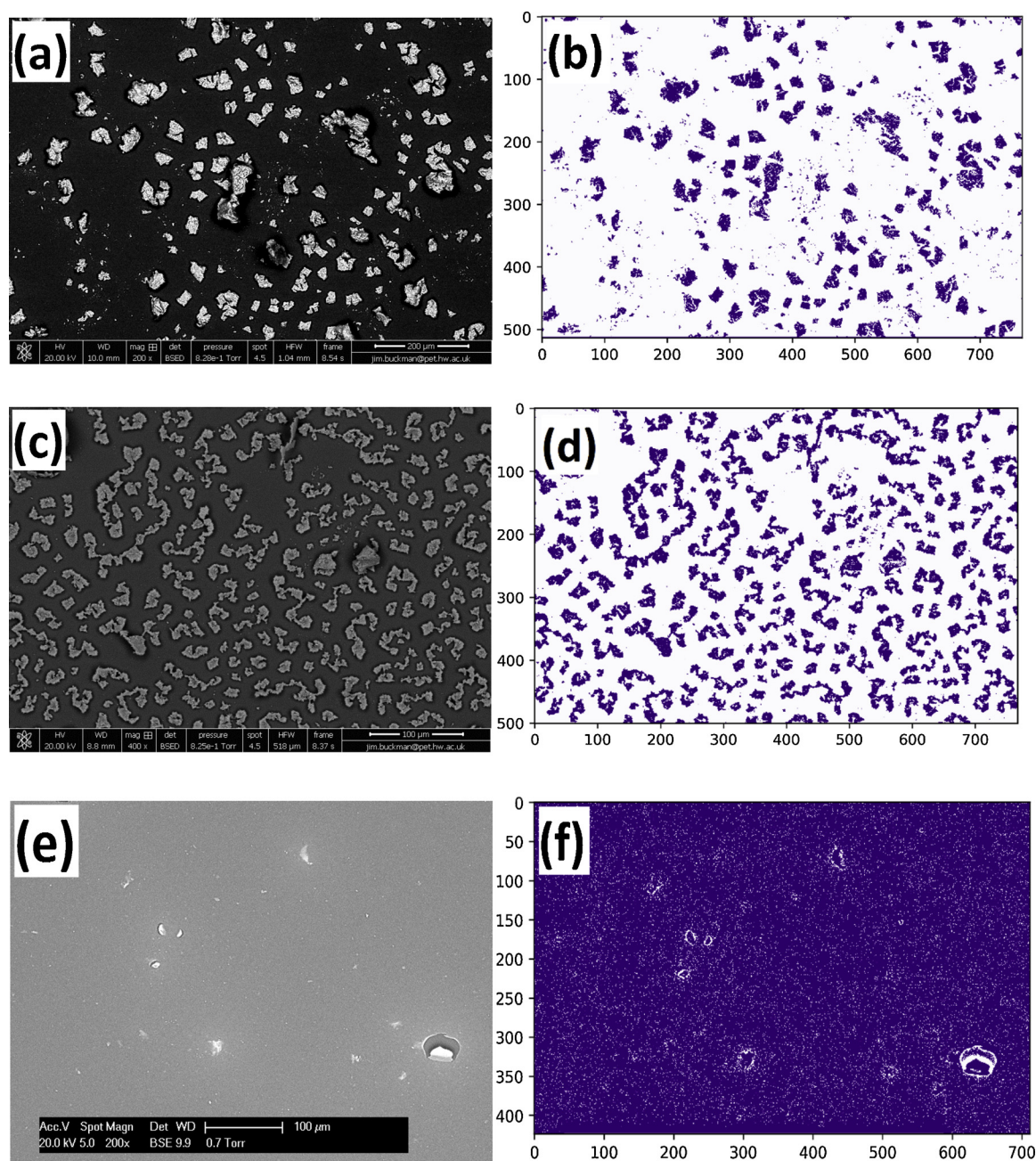
Fig. 4. A variety of coating quality and coverage were observed as a result of the parameter settings shown in Table 1. Adaptive or Otsu global thresholding was chosen by eye by comparing the threshold image with the SEM image. The SEM images are shown on the left and the threshold images on the right. The threshold images include x and y axis in pixel units (a) WT10 (b) WT10 - Otsu global thresholding (c) WT5 (d) WT5 - Otsu global thresholding (e) WT2 (f) WT2 - Adaptive thresholding.

and green dotted line show the low and high settings effect respectively on the selected parameter shown on the x-axis of the graph. The two lines show how at high and low settings, how the setting of the interacting parameter changes its effect on the given response.

3.1.2. Band gap response

A range of band gaps were recorded for the fifteen PB experiments (Fig. 2). The PB design was converted to a two factor full factorial design and an interaction effect between calcination temperature and holding time was found (Fig. 3c). Increasing the calcination temperature resulted in higher band gap values (Fig. 3b). An increase in the holding time decreased the band gap recorded and had less of an effect relative to calcination temperature (Fig. 3a,b). The interaction main effects plot shown in Fig. 3c showed that at high calcination

temperatures, an interaction effect with holding time, where at calcination temperature 650 °C, both 10 and 120 min hold times yielded the same mean band gap. Whilst at calcination temperature 250 °C, 10 and 120 min hold times yielded a larger and smaller band gap, respectively. This shows that the dominating effect is that of calcination temperature at high settings, where holding time has little effect as the temperature increases. It is proposed that the change in band gap is from the kinetics of TiO_2 phase change being dependent on temperature at higher calcination temperatures. Momeni et al also observed an increase in band gap recorded for N doped TiO_2 films with increasing calcination temperature [9,10]. The design reported here started with experimental points at 250 °C which yielded amorphous TiO_2 with low band gap values in the visible light region (≈ 2.0 eV). At lower calcination temperature (450 °C), the holding time showed a greater difference in effect
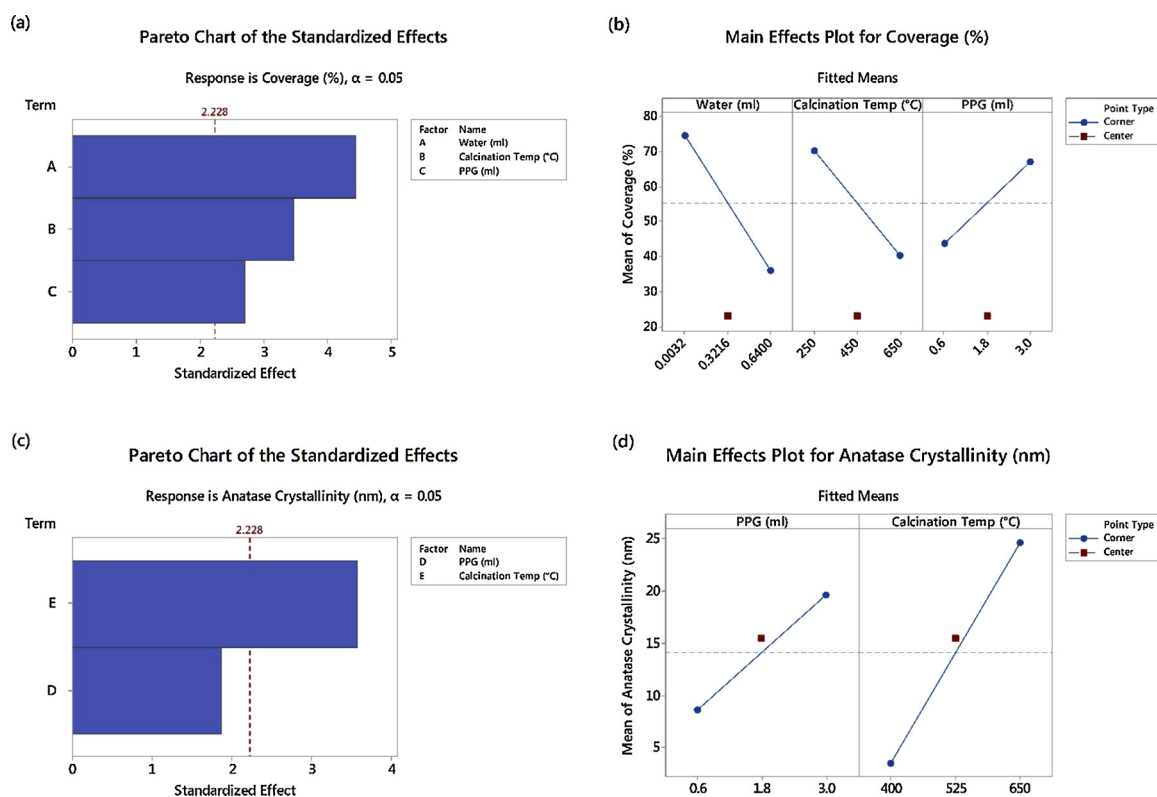
Fig. 5. (a) Pareto chart of effects from full factorial model showing significance of amount of water, PPG and calcination temperature on the % coverage response. No interaction effects were found. (b) Main effects plot showing effect amount of water, PPG and calcination temperature on the coverage response. (c) Pareto chart of effects showing significance of calcination temperature and amount PPG used on the crystallinity of the anatase phase response. (d) Main effects plot showing effect of the calcination temperature and amount of PPG used on the crystallinity response.
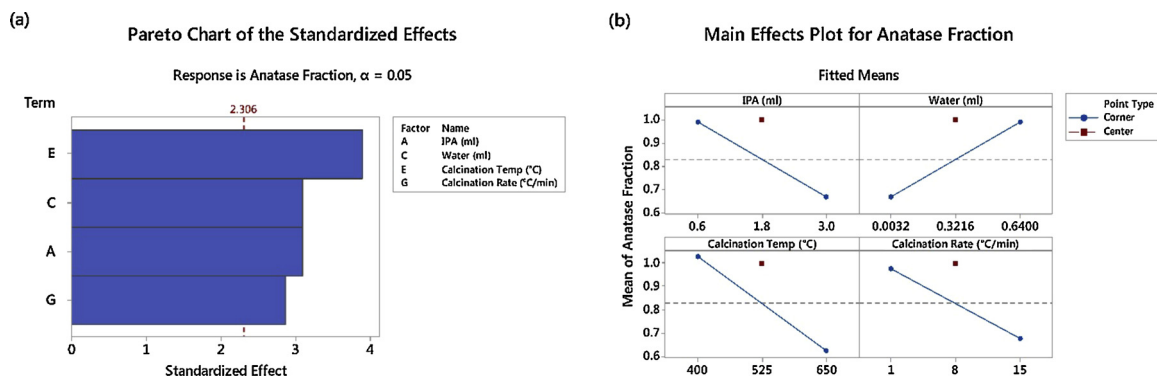

Fig. 6. (a) Pareto chart of effects showing significance of amount IPA, water and the calcination temperature and heating ramp on the ratio anatase:rutile response. (b) Main effects plot showing effects of IPA, water and the calcination temperature and heating ramp on the ratio anatase:rutile response.

between short holding times (10 min) versus long holding times (120 min). Longer holding times would encourage increased crystallinity at a set calcination temperature and this has been shown to lower the observed band gap [11].

3.1.3. Coverage response

Machine vision provides a powerful tool for analysing images [42]. SEM images were taken of the coated glass slides and a Python script was written to perform manual global, Otsu global and adaptive thresholding – see supplementary info for the script used.

The PB design yielded a variety of coatings ranging from poor clumped coatings (Fig. 4a,b) to a thin uniform film, using WT2 settings, with high surface coverage of 98.94% using adaptive thresholding (Fig. 4f). The Otsu method worked the best out of the three Python methods employed as it showed the greatest variation

(Otsu$_{\sigma^2}$ = 432.67, Adaptive$_{\sigma^2}$ = 227.91 and Manual$_{\sigma^2}$ = 35.15) and showed the best estimation of coverage when compared by eye with the original images (Table 2). The Python script yielded satisfactory thresholding results, although it must be noted that confirmation of the thresholding still required confirmation by eye.

The amount of water showed the greatest effect on the percentage coverage with an increase in water decreasing the percentage coverage (Fig. 5a,b). Rezaee et al found that for the preparation of yttria-doped zirconia sol-gels, the coating showed more cracking by SEM when excess water was used [43]. Using more water for the preparation of the sol-gels may have caused agglomeration, as water was added in one portion that may have resulted in very fast and complete hydrolysis and polycondensation producing agglomerates. Moemeni et al reported increased cracking with higher calcination temperature and proposed this was due to differences in expansion co-efficients between the coating
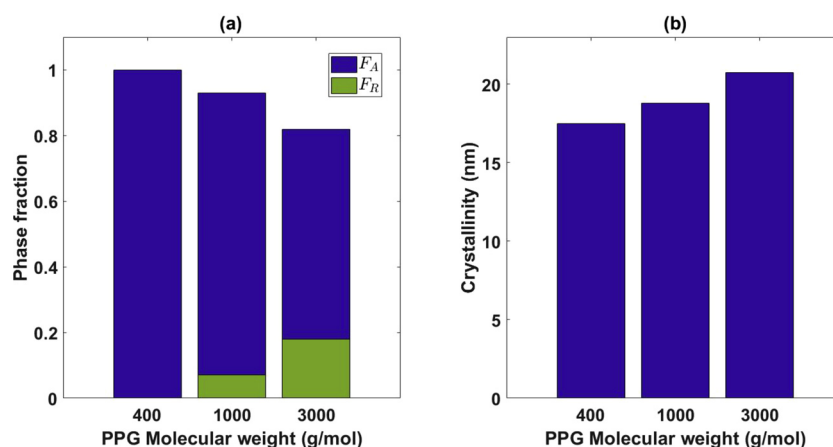
Fig. 7. Effect molecular weight PPG on: (a) phase fraction (b) crystallinity of anatase phase.
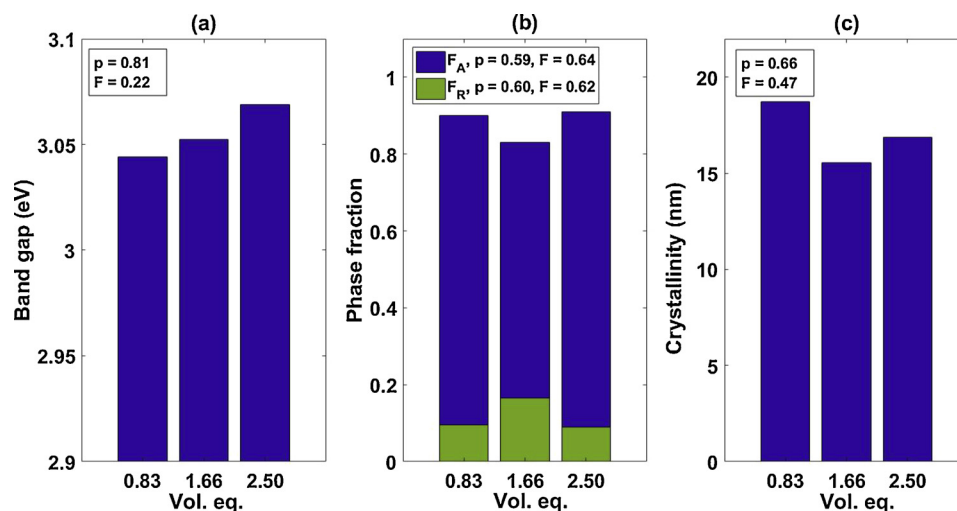

Fig. 8. Effect of volume equivalents PPG on (a) band gap (b) anatase phase fraction (F_A) and rutile phase fraction (F_R) (c) crystallinity.
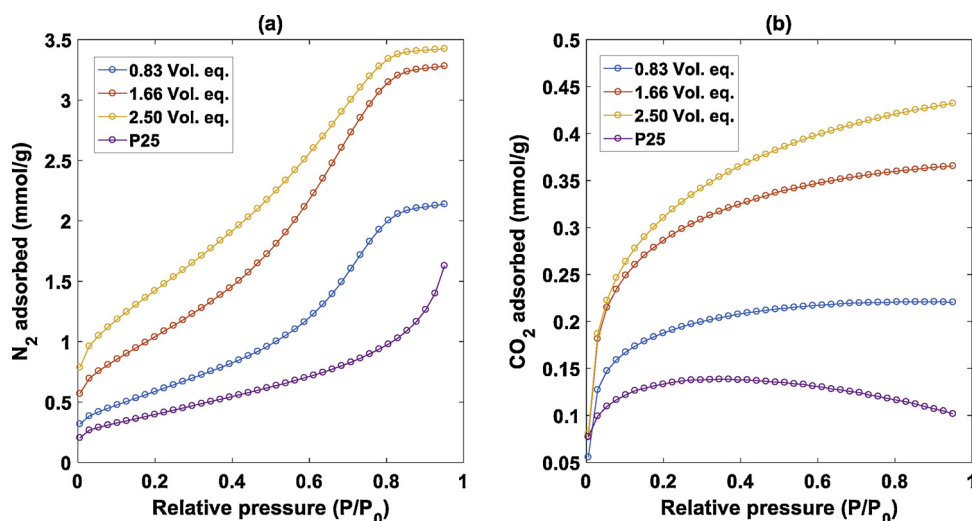

Fig. 9. N_2 (a) and CO_2 (b) adsorbtion isotherms for the samples prepared with different volume equivalents of PPG and reference P25 TiO_2.

and support used [9,10].

Fig. 5d shows that an increase in annealing temperature also increased the crystallinity, as high temperatures could have overcome the surface tension of the coating leading to the formation of cracks. The opposite relationship was found for the amount of PPG used, where the

percentage coverage increased with an increase in amount PPG used. Calderon-Morenoa et al showed that using high molecular weight polyethylene glycol (PEG) resulted in homogenous films prepared by TiO_2 sol-gels [44]. The presence of high molecular weight PEG may have bound the coatings better on calcination as the polycondensed

Table 3
BET specific surface area (SSA), pore volume (VTot) and maximum CO_2 adsorption recorded for reference P25 TiO_2 [42] and TiO_2 catalysts prepared using 0.83, 1.66 and 2.50 vol equivalents PPG.

Catalyst	SSA (m^2/g)	V_{Tot} (m^3/g)	Max CO_2 adsorption (mmol/g)
P25	53.31	0.090	0.17
0.83 Vol. eq.	50.01	0.074	0.22
1.66 Vol. eq.	87.69	0.113	0.36
2.50 Vol. eq.	111.91	0.118	0.43

chains were converted to TiO_2 crystals.

3.1.4. Crystallinity response

The PB design could be converted to a two factor full factorial design for the crystallinity of the anatase phase response as only one factor, calcination temperature, was found to have a statistically significant effect on the crystallinity response (Fig. 5c). Amount of PPG was included as it improved the model by increasing the random distribution of residual vs. fitted values. It is potentially an interesting factor to consider in future studies. Again, as per the reasons given when discussing the ratio of anatase to rutile response (Section 3.1.5), the temperature of the low design points and midpoints were taken at 400 and 525 °C, respectively. The experimental design showed an increase in the crystallinity with higher calcination temperature and the amount of PPG used for the preparation of the sol-gel. An increase in calcination temperature has been reported to yield higher TiO_2 crystallinity [9,10,12–15].

The amount of PPG used may have slowed the growth of the crystals and yielded high crystallinity as it has a high affinity with water. This would have slowed down the initial evaporation rate of water. Similar reasons were given by Mosén et al who investigated the effects of polyethylene glycol (PEG) on the crystallinity of spray dried lactose and PEG mixtures [45]. In addition, more PPG could have offered more nucleation sites for the crystallization of TiO_2 [45].

3.1.5. Phase ratio response

The PB design showed that the amount of IPA and water used for the preparation for the sol-gel along with the calcination temperature and heating rate were statistically significant effects on the ratio of anatase to rutile phase (Fig. 6a). The results presented use the amount of anatase as a response, if rutile was used the same factors would have been statistically significant and the main effects plots would have been the inverse of that shown in Fig. 6b. It can be seen that an increase in the

amount of IPA, calcination temperature and heating rate favored a lower ratio of anatase, whilst the opposite was true for the amount of water used (Fig. 6b). The effect of temperature on the phase change from anatase to rutile is well documented [9,10,17–22]. It is also worth noting that according to Hanoar et al, the transformation of the anatase to rutile phase is a complex process that could include the following factors: particle size, particle shape (aspect ratio), surface area, atmosphere, volume of sample, nature of sample container, heating rate, and inclusion of impurities [21]. The inclusion of organic crystallization impurities in this work may have resulted from the inclusion of IPA in the crystals formed. Ocana et al showed that the inclusion of organic impurities encouraged the formation of the rutile phase on the catalyst's surface [46].

3.2. Optimisation of best design point

3.2.1. Optimal design point

Due to the nature of the wide design space explored for a PB design, there is a high probability that one of the points will yield a useful response. For this PB design, WT2 showed a favorable percentage coverage (98%), band gap (3.35 eV), crystallinity anatase phase (28.01 nm) and anatase : rutile ratio (25:75). WT2's properties would be of interest to benchmark against the commercially available P25 TiO_2 photocatalyst. Using this point's settings (WT2, Table 1), the effects of PPG molecular weight and volume equivalents were investigated and are presented in the next section.

3.2.2. Effect of PPG molecular weight and volume used

Building on the PB design's results and using the best design point WT2, the coating process was further investigated for the effect of the molecular weight and amount of the PPG used. PPG with molecular weights: 400, 1000 and 3000 were tested. High molecular weight PPG costs more, and therefore, lower molecular weights were investigated to reduce the cost of the sol-gel preparation. Five volume equivalents PPG relative to the starting volume of titanium (IV) n-butoxide (0.6 ml) was used for the preparation of WT2. To optimise the amount of PPG used, 0.83, 1.66 and 2.50 vol equivalents PPG relative to the starting reagent titanium (IV) n-butoxide were investigated for the preparation of TiO_2 sol-gel. When the molecular weight of PPG increased from 400 to 3000, using five volume equivalents PPG, the rutile:anatase ratio increases (Fig. 7). The biggest increase in rutile phase observed for PPG 3000. Some rutile was observed for PPG 1000 and this does warrant further investigation in the future. The anatase crystalline size increased with higher molecular weight (Fig. 7). The mean values recorded for band gap, fraction phase and crystallinity of the anatase phase using 0.83,
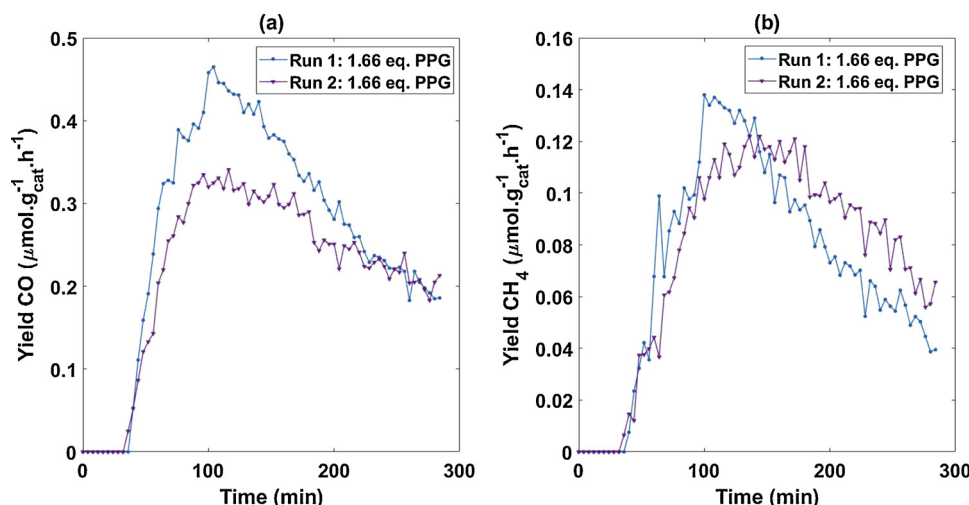

Fig. 10. CO_2 photoreduction reaction repeat tests using 1.66 vol equivalents PPG for production of (a) CO and (b) CH_4.
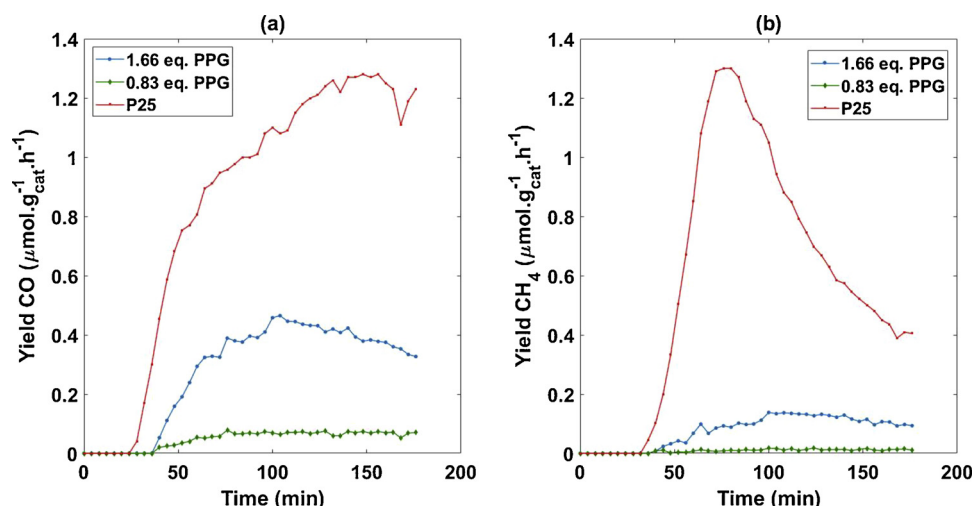
Fig. 11. CO_2 photoreduction reaction tests comparing gauge 20 mesh coated with sol-gel using 1.66 and 0.83 vol equivalents PPG for production of (a) CO and (b) CH_4.

Table 4

Comparison of band gap, crystallinity anatase and rutile between reference P25 TiO_2 [42], TiO_2 catalyst prepared using 1.66 and 0.83 vol equivalents PPG.

Catalyst	Anatase crystallinity (nm)	Rutile crystallinity (nm)	Band gap (eV)
P25	12.6	14.2	3.20
1.66 eq.	16.2	175.1	3.06
0.83 eq.	17.6	163.6	3.04

1.66 and 2.50 vol equivalents of PPG is shown in Fig. 8. Although a small increase was observed for band gap when increasing volume equivalents of PPG, a one way analysis of variance (ANOVA) indicated that there was no statistically significant difference in means for band gap, anatase phase, rutile phase and crystallinity of anatase phase. The *p*-value (p) is the probability that the *F*-statistic (F) is larger than the computed test-statistic value. A *p*-value that is more than the significance level (α), in this case α = 0.05, indicates that the means are not significantly different (Fig. 8). This supports the output from the PB model, where the volume of PPG had no statistically significant effect on these responses.

Type IV N_2 adsorption isotherms were observed for the TiO_2 samples prepared using 0.83, 1.66 and 2.50 vol equivalents of PPG, whilst P25 TiO_2 exhibited a Type II adsorption isotherm (Fig. 9a). The type IV adsorption isotherms of the 0.83, 166 and 2.50 vol equivalent PPG samples indicated the solids were mesoporous [47]. Type I CO_2 adsorption isotherms were observed for the TiO_2 samples prepared using 0.83, 1.66 and 2.50 vol equivalents PPG and for P25 TiO_2 (Fig. 9b). The samples prepared using 0.83, 1.66 and 2.50 vol equivalents PPG increased N_2 and CO_2 adsorption compared to P25 TiO_2 could be explained by the mesoporous solids yielding a higher surface area versus the microporous P25 TiO_2. The surface area and maximum CO_2 adsorbed increased with volume equivalents of PPG used (Table 3). CO_2 adsorption capacity increased with increasing pressure with a maximum found at 0.95 P/P_0 for the TiO_2 samples prepared using 0.83, 1.66 and 2.50 vol equivalents PPG, whilst the CO_2 adsorption capacity decreased with increasing pressure for P25 TiO_2 with a maximum capacity at 0.30 P/P_0. For the 0.83, 1.66 and 2.50 vol equivalent PPG samples, an increase in CO_2 adsorption capacity correlated with an increase in photocatalytic activity for both CO and CH_4 production (Fig. 11). This is likely because a higher CO_2 adsorption capacity would increase the probability of CO_2 photoreduction as CO_2 would be in closer proximity to active sites, especially the (001) anatase facets, on the catalyst's surface [48].

3.2.3. CO_2 photoreduction results

The reaction was attempted twice as Run 1 and Run 2 using 1.66 equivalents of PPG (Fig. 10). For Run 1 and 2 using 1.66 vol equivalents PPG, similar trends were observed for the production of CO and CH_4, with Run 1 producing more CO initially and later matching Run 2′s CO production. This was confirmed with paired two sample t-tests, where if the calculated *t*-statistic is greater than the critical value (cv) of the student's *t*-distribution table, using the degrees of freedom (df) and significance level (α), the means are significantly different. Run 1 and 2 yielded statistically equal CH_4 production over the entire time range (α = 0.05, df = 142, t-statistic = -0.5735, cv = 2.576). Run 1 and 2 yielded statistically equal CO production from 204 min (α = 0.05, df = 40, t-statistic = 0.9016, cv = 2.704). The coated meshes prepared by the sol-gel method were compared to a mesh coated with reference P25 TiO_2. For both CO and CH_4 production, P25 TiO_2 coated mesh performed better (Fig. 11). The difference in performance could be due to the differences in crystallinity and band gap (Table 4). Increase in band gap has been reported with decreasing crystal size, where the rutile crystallite size for the 1.66 and 0.83 equivalents PPG samples having much larger rutile and slightly bigger anatase crystallite sizes compared to P25 [5,49]. The larger band gap and resulting increase in the number of photons generated by P25 would favor CO_2 photoreduction [3]. The difference in production could also be due to the difference in coating methods used where the P25 TiO_2 was applied to the stainless steel mesh using a slurry coating method versus a dip coating method for the optimised samples. There are examples in the literature that report the influence of carbon impurities introduced during the catalyst's preparation and/or from the coating procedure on the production of both CH_4 and CO [50–53]. Future work would include investigating the effects of the coating procedure on the potential false positive production of CH_4 and CO. It is also important to note that this was a benchmarking exercise where the sol-gel process was developed to yield catalyst properties that were benchmarked against P25 TiO_2. In addition, although not as efficient as P25, the advantage this sol-gel procedure is its coating flexibility, where it could be potentially applied to different supports on a large scale using a spray paint process. Mesh coated with 1.66 vol equivalents PPG produced more CO and CH_4 compared to the mesh coated with 0.83 vol equivalents PPG. This is most likely due to the synergistic effects of rutile and anatase where an increase in rutile phase exhibits improved photocatalytic activity [6]. The 1.66 vol equivalents PPG sample had 18.1% rutile phase and the 0.83 vol equivalents PPG sample had less with 11.8% rutile phase. In addition, the 1.66 vol equivalents sample had a higher CO_2 adsorption capacity (0.36 mmol/g) compared to the 0.83 vol equivalents

sample (0.22 mmol/g) where a higher probability exists for the reaction to occur if CO_2 is adsorbed onto the catalyst's surface (Table 3).

4. Conclusions

A systematic approach using a PB design was used to efficiently screen seven sol-gel parameters towards a catalyst coating with a high coverage and useful properties for CO_2 photoreduction. It was possible using a DOE methodology to develop a sol-gel procedure that could tune band gap, coverage, crystallinity and anatase:rutile ratio for CO_2 photoreduction. Moreover, the PB design yielded similar observations made in several publications in as few as fifteen experiments. The best design point (WT2) was further optimized to use less PPG. The lower activity of the sol-gel prepared catalyst coatings to P25 was likely due to larger crystallite size, lower band gap values and the potential effects of false positives from the different coating procedures used. This PB design and protocols developed could be employed towards a variety of catalyst coatings with a wide range of properties.

Acknowledgments

Appendix A. Supplementary data

Supplementary material related to this article can be found, in the online version, at doi:https://doi.org/10.1016/j.apcatb.2018.07.018.

References

[1] L. Yuan, Y.-J. Xu, Photocatalytic conversion of CO2 into value-added and renewable fuels, Appl. Surf. Sci. 342 (2015) 154–167.

[2] M.-Q. Yang, Y.-J. Xu, Photocatalytic conversion of CO2 over graphene-based composites: current status and future perspective, Nanoscale Horiz. 1 (2016) 185–200.

[3] O. Ola, M. Maroto-Valer, Review of material design and reactor engineering on TiO2 photocatalysis for CO2 reduction, J. Photochem. Photobiol. C 24 (2015) 16–42.

[4] A. Olivo, E. Ghedini, M. Signoretto, M. Compagnoni, I. Rossetti, Liquid vs. Gas phase CO2 photoreduction process: which Is the effect of the reaction medium? Energies 10 (2017) 1394.

[5] K. Kočí, L. Obalová, L. Matějová, D. Plachá, Z. Lacný, J. Jirkovský, O. Šolcová, Effect of TiO2 particle size on the photocatalytic reduction of CO2, Appl. Catal. B 89 (2009) 494.

[6] P. Bouras, E. Stathatos, P. Lianos, Pure versus metal-ion-doped nanocrystalline titania for photocatalysis, Appl. Catal. B 73 (2007) 51–59.

[7] I. Ganesh, Effects of phosphorous-doping on energy band-gap, structural, surface, and photocatalytic characteristics of emulsion-based sol-gel derived TiO2 nano-powder, Appl. Surf. Sci. 414 (2017) 277–291.

[8] E.M. Samsudin, S.B. Abd hamid, effect of band gap engineering in anionic-doped TiO2 photocatalyst, Appl. Surf. Sci. 391 (2017) 326–336.

[9] M. Momeni, H. Saghafian, F. Golestani-Fard, N. Barati, A. Khanahmadi, Effect of SiO2 addition on photocatalytic activity, water contact angle and mechanical stability of visible light activated TiO2 thin films applied on stainless steel by a sol gel method, Appl. Surf. Sci. 392 (2017) 80–87.

[10] M. Momeni, F. Golestani-Fard, H. Saghafian, N. Barati, A. Khanahmadi, Development of visible light activated TiO2 thin films on stainless steel via sol spraying with emphasis on microstructural evolution and photocatalytic activity, Appl. Surf. Sci. 357 (2015) 1902–1910.

[11] H. Albetran, B.H. O'Connor, I.M. Low, Effect of calcination on band gaps for electrospun titania nanofibers heated in air–argon mixtures, Mater. Des. 92 (2016) 480–485.

[12] P. Kajitvichyanukul, J. Ananpattarachai, S. Pongpom, Sol–gel preparation and properties study of TiO2 thin film for photocatalytic reduction of chromium(VI) in photocatalysis process, Sci. Technol. Adv. Mater. 6 (2005) 352–358.

[13] C.P. Lin, H. Chen, A. Nakaruk, P. Koshy, C.C. Sorrell, Effect of annealing temperature on the photocatalytic activity of TiO2 thin films, Energy Procedia 34 (2013) 627–636.

[14] L.R.Paj. Matousek, Preparation of TiO2 sol-gel layers on glass, Ceramics − Silikáty 47 (1) (2003) 28–31.

[15] W.-K. Wang, J.-J. Chen, X. Zhang, Y.-X. Huang, W.-W. Li, H.-Q. Yu, Self-induced synthesis of phase-junction TiO2 with a tailored rutile to anatase ratio below phase transition temperature, Sci. Rep. 6 (2016) 20491.

[16] M. Fallah, M.-R. Zamani-Meymian, R. Rahimi, M. Rabbani, Effect of annealing treatment on electrical and optical properties of Nb doped TiO2 thin films as a TCO prepared by sol–gel spin coating method, Appl. Surf. Sci. 316 (2014) 456–462.

[17] T.B. Ghosh, S. Dhabal, A.K. Datta, On crystallite size dependence of phase stability of nanocrystalline TiO2, J. Appl. Phys. 94 (2003) 4577–4582.

[18] G. Li, L. Li, J. Boerio-Goates, B.F. Woodfield, High purity anatase TiO2 nanocrystals: near room-temperature synthesis, grain growth kinetics, and surface hydration chemistry, J. Am. Chem. Soc. 127 (2005) 8659–8666.

[19] M. Hirano, C. Nakahara, K. Ota, O. Tanaike, M. Inagaki, Photoactivity and phase stability of ZrO2-doped anatase-type TiO2 directly formed as nanometer-sized particles by hydrolysis under hydrothermal conditions, J. Solid State Chem. 170 (2003) 39–47.

[20] V. Raj, M.S. Mumjitha, Formation and surface characterization of nanostructured Al2O3-TiO2 coatings, Bull. Mater. Sci. 37 (2014) 1411–1418.

[21] D.A.H. Hanaor, C.C. Sorrell, Review of the anatase to rutile phase transformation, J. Mater. Sci. 46 (2010) 855–874.

[22] D. Regonini, A. Jaroenworaluck, R. Stevens, C.R. Bowen, Effect of heat treatment on the properties and structure of TiO2nanotubes: phase composition and chemical composition, Surf. Interface Anal. 42 (2010) 139–144.

[23] N. Negishi, K. Takeuchi, Preparation of TiO2 thin film photocatalysts by dip coating using a highly viscous solvent, J. Sol-Gel Sci. Technol. 22 (2001) 23–31.

[24] A.A. Daniyan, L.E. Umoru, B. Olunlade, Preparation of nano-TiO&sub2&/sub& thin film using spin coating method, J. Miner. Mater. Charact. Eng. 01 (04) (2013) 7.

[25] A. Elfanaoui, E. Elhamri, L. Boulkaddat, A. Ihlal, K. Bouabid, L. Laanab, A. Taleb, X. Portier, Optical and structural properties of TiO2 thin films prepared by sol–gel spin coating, Int. J. Hydrogen Energy 36 (2011) 4130–4133.

[26] W. Zhang, J. Bai, Synthesis and photocatalytic properties of porous TiO2 films prepared by ODA/sol–gel method, Appl. Surf. Sci. 258 (2012) 2607–2611.

[27] M. Sleiman, D. Vildozo, C. Ferronato, J.-M. Chovelon, Photocatalytic degradation of azo dye metanil yellow: optimization and kinetic modeling using a chemometric approach, Appl. Catal. B 77 (2007) 1–11.

[28] R. Carrera-Cerritos, C. Ponce de Leon, J. Ledesma-Garcia, R. Fuentes-Ramirez, L.G. Arriaga, Full factorial design applied to the synthesis of Pd-Ag nanobars by the polyol method and the perspective for ethanol oxidation, RSC Adv. 4 (2014) 16632–16640.

[29] R. Saada, O. AboElazayem, S. Kellici, T. Heil, D. Morgan, G.I. Lampronti, B. Saha, Greener synthesis of dimethyl carbonate using a novel tin-zirconia/graphene nanocomposite catalyst, Appl. Catal. B 226 (2018) 451–462.

[30] P.J. Schmitz, R.J. Kudla, A.R. Drews, A.E. Chen, C.K. Lowe-Ma, R.W. McCabe, W.F. Schneider, C.T. Goralski, NO oxidation over supported Pt: impact of precursor, support, loading, and processing conditions evaluated via high throughput experimentation, Appl. Catal. B 67 (2006) 246–256.

[31] A. Ekebergh, C. Lingblom, P. Sandin, C. Wenneras, J. Martensson, Exploring a cascade heck-suzuki reaction based route to kinase inhibitors using design of experiments, Org. Biomol. Chem. 13 (2015) 3382–3392.

[32] J. Marbach, B. Nornberg, A.F. Rahlf, G.A. Luinstra, Zinc glutarate-mediated copolymerization of CO2 and PO - parameter studies using design of experiments, Catal. Sci. Technol. 7 (2017) 2897–2905.

[33] P. Chang, A. Aillerie, M. Kosmala, S. Pellegrini, T. Bousquet, M. Bigan, L. Pelinski, Catalytic one-pot microwave assisted synthesis of 4-azapodophyllotoxin derivatives and rational design of experiment, New J. Chem. 39 (2015) 8236–8239.

[34] P.J. Wojcik, L. Pereira, R. Martins, E. Fortunato, Statistical mixture design and multivariate analysis of inkjet printed a-WO3/TiO2/WOX electrochromic films, ACS Comb. Sci. 16 (2014) 5–16.

[35] L. Sun, T. An, S. Wan, G. Li, N. Bao, X. Hu, J. Fu, G. Sheng, Effect of synthesis conditions on photocatalytic activities of nanoparticulate TiO2 thin films, Sep. Purif. Technol. 68 (2009) 83–89.

[36] D.L. Marchisio, F. Omegna, A.A. Barresi, P. Bowen, Effect of mixing and other operating parameters in sol − gel processes, Ind. Eng. Chem. Res. 47 (2008) 7202–7210.

[37] S.A. Ansari, M.H. Cho, Simple and large scale construction of MoS(2)-g-C(3)N(4) heterostructures using mechanochemistry for High performance electrochemical supercapacitor and visible light photocatalytic applications, Sci. Rep. 7 (2017) 43055.

[38] M.M. Khan, S.A. Ansari, D. Pradhan, M.O. Ansari, D.H. Han, J. Lee, M.H. Cho, Band gap engineered TiO2 nanoparticles for visible light induced photoelectrochemical and photocatalytic studies, J. Mater. Chem. A 2 (2014) 637–644.

[39] L.E.A. Harold, P. Klug, X-Ray Diffraction Procedures: For Polycrystalline and Amorphous Materials, John Wiley & Sons, New York, 1959.

[40] R.A. Spurr, H. Myers, Quantitative analysis of anatase-rutile mixtures with an X-ray diffractometer, Anal. Chem. 29 (1957) 760–762.

[41] S. Lowell, J.E. Shields, M.A. Thomas, M. Thommes, Micropore Analysis, Characterization of Porous Solids and Powders: Surface Area, Pore Size and Density, Springer, Netherlands, Dordrecht, 2004, pp. 129–156.

[42] X.-c. Yuan, L.-s. Wu, Q. Peng, An improved Otsu method using the weighted object variance for defect detection, Appl. Surf. Sci. 349 (2015) 472–484.

[43] S. Rezaee, G. Rashed, M.A. Golozar, Effect of Water/Alkoxide molar ratio on the synthesis process and electrochemical behavior of yttria-doped zirconia sol-gel films, Iran. J. Oil Gas Sci. Technol. 2 (2013) 57–70.

[44] J.M. Calderon-Moreno, S. Preda, L. Predoana, M. Zaharescu, M. Anastasescu, M. Nicolescu, M. Stoica, H. Stroescu, M. Gartner, O. Buiu, M. Mihaila, B. Serban, Effect of polyethylene glycol on porous transparent TiO2 films prepared by sol–gel method, Ceram. Int. 40 (2014) 2209–2220.

[45] K. Mosén, K. Bäckström, K. Thalberg, T. Schaefer, A. Axelsson, H.G. Kristensen, The apparent plasticizing effect of polyethylene glycol (PEG) on the crystallinity of spray dried lactose/PEG composites, Eur. J. Pharm. Biopharm. 64 (2006) 206–211.

[46] M. Ocana, J.V. Garcia-Ramos, C.J. Serna, J. Am. Ceram. Soc. 75 (1992) (2010).

[47] P. Schneider, Adsorption isotherms of microporous-mesoporous solids revisited, Appl. Catal. A 129 (1995) 157–165.

[48] X. Chang, T. Wang, J. Gong, CO2 photo-reduction: insights into CO2 activation and reaction on surfaces of photocatalysts, Energy Environ. Sci. 9 (2016) 2177–2196.

[49] S. Wang, S. Lin, D. Zhang, G. Li, M.K.H. Leung, Controlling charge transfer in quantum-size titania for photocatalytic applications, Appl. Catal. B 215 (2017) 85–92.

[50] A. Pougin, M. Dilla, J. Strunk, Identification and exclusion of intermediates of photocatalytic CO2 reduction on TiO2 under conditions of highest purity, PCCP 18 (2016) 10809–10817.

[51] J.C.S. Wu, C.-W. Huang, In situ DRIFTS study of photocatalytic CO2 reduction under UV irradiation, Front. Chem. Eng. China 4 (2010) 120–126.

[52] T. Yui, A. Kan, C. Saitoh, K. Koike, T. Ibusuki, O. Ishitani, Photochemical reduction of CO2 using TiO2: effects of organic adsorbates on TiO2 and deposition of Pd onto TiO2, ACS Appl. Mater. Interfaces 3 (2011) 2594–2600.

[53] A. Cybula, M. Klein, A. Zaleska, Methane formation over TiO2-based photocatalysts: reaction pathways, Appl. Catal. B 164 (2015) 433–442.